Science of the Total Environment 864 (2023) 161194

Contents lists available at ScienceDirect

Science of the Total Environment

journal homepage: www.elsevier.com/locate/scitotenv

Degradation of diclofenac and 4-chlorobenzoic acid in aqueous solution by cold atmospheric plasma source

Amit Kumar [a,b,*], Nikola Škoro [a], Wolfgang Gernjak [c,d], Olivera Jovanović [a], Anđelija Petrović [a], Suzana Živković [e], Elisabeth Cuervo Lumbaque [c], Maria José Farré [c], Nevena Puač [a]

[a] Institute of Physics, University of Belgrade, Pregrevica 118, 11080 Belgrade, Serbia
[b] Universitat de Girona, 17003 Girona, Spain
[c] Catalan Institute for Water Research (ICRA), 17003 Girona, Spain
[d] Catalan Institution for Research and Advanced Studies (ICREA), 08010 Barcelona, Spain
[e] Institute for Biological Research "Siniša Stanković", University of Belgrade, Bulevar despota stefana 142, 11060, Serbia

HIGHLIGHTS

- Multi-pin APPJ utilized to treat DCF and pCBA in aqueous solution.
- Shown efficient removal of contaminants with large plasma/contaminant surface ratio
- Energy yield determined using power deposited to discharge in contact with sample
- A multi-pin APPJ with recirculation system allows for scalability.

GRAPHICAL ABSTRACT

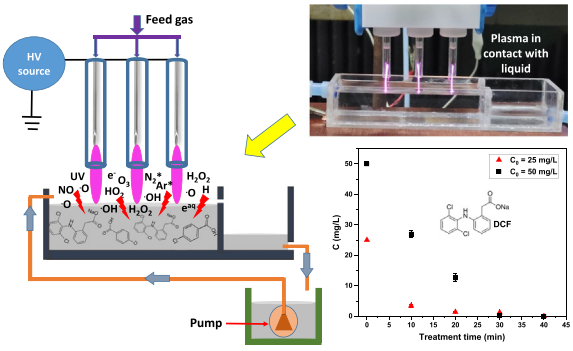

ARTICLE INFO

Editor: Yifeng Zhang

Keywords:
Cold atmospheric plasma
Plasma characterization
Degradation of pharmaceutical and industrial chemical

ABSTRACT

In this study, cold atmospheric plasma (CAP) was explored as a novel advanced oxidation process (AOP) for water decontamination. Samples with high concentration aqueous solutions of Diclofenac sodium (DCF) and 4-Chlorobenzoic acid (pCBA) were treated by plasma systems. Atmospheric pressure plasma jets (APPJs) with a 1 pin-electrode and multi-needle electrodes (3 pins) configurations were used. The plasma generated using argon as working gas was touching a stationary liquid surface in the case of pin electrode-APPJ while for multi-needle electrodes-APPJ the liquid sample was flowing during treatment. In both configurations, a commercial RF power supply was used for plasma ignition. Measurement of electrical signals enabled precise determination of power delivered from the plasma to the sample. The optical emission spectroscopy (OES) of plasma confirmed the appearance of excited reactive species in the plasma, such as hydroxyl radicals and atomic oxygen which are considered to be key reactive species in AOPs for the degradation of organic pollutants. Treatments were conducted with two different volumes (5 mL and 250 mL) of contaminated water samples. The data acquired allowed calculation of degradation efficiency and energy yield for both plasma sources. When treated with pin-APPJ, almost complete degradation of 5 mL DCF occurred in 1 min with the initial concentration of 25 mg/L and 50 mg/L, whereas 5 mL pCBA almost degraded in 10 min at the initial concentration of 25 mg/L and 40 mg/L. The treatment results with multi-needle electrodes system confirmed that DCF almost completely degraded in 30 min and pCBA degraded about 24 % in 50 min. The maximum

* Corresponding author at: Institute of Physics, University of Belgrade, Pregrevica 118, 11080 Belgrade, Serbia.
E-mail address: amit@ipb.ac.rs (A. Kumar).

http://dx.doi.org/10.1016/j.scitotenv.2022.161194
Received 5 October 2022; Received in revised form 21 December 2022; Accepted 21 December 2022
Available online 27 December 2022
0048-9697/© 2022 The Authors. Published by Elsevier B.V. This is an open access article under the CC BY-NC license (http://creativecommons.org/licenses/by-nc/4.0/).

calculated energy yield for 50 % removal was 6465 mg/kWh after treatment of 250 mL of DCF aqueous solution utilizing the plasma recirculation technique. The measurements also provided an insight to the kinetics of DCF and pCBA degradation. Degradation products and pathways for DCF were determined using LC-MS measurements.

1. Introduction

Many pharmaceutical and other industrial organic chemical substances have been recognized as emerging persistent organic micropollutants (OMPs) and are frequently found in trace concentrations (ranging from ngL^{-1} and μgL^{-1}) in aquatic bodies (Arslan et al., 2017; Ebele et al., 2017; Patel et al., 2019). It is estimated that several tons of pharmaceuticals, for example, >100,000 tons of pharmaceutical items, are consumed globally each year, inflicting harm to our ecosystem (Kot-Wasik et al., 2007; Wilkinson et al., 2022). Pharmaceutical and other industrial chemicals are discharged to the environment from a wide range of sources, including industry, hospitals and households. Pharmaceuticals are detected in the environment through a variety of channels due to a lack of proper wastewater treatment technologies; they all share the characteristics of providing a considerable threat to public health or the environment, as well as being extremely resistant to traditional wastewater treatment techniques (Arslan et al., 2017; Eggen et al., 2014; Khan et al., 2020). Certain organizations, such as the European Union (EU) and the United States Environmental Protection Agency (USEPA), establishing strict quality criteria for wastewater discharge; yet, various nations and industries are following that (Sathishkumar et al., 2020; Schellenberg et al., 2020). The previous review article by various authors offers thorough information regarding pharmaceutical classification, source and regulations, as well as the impact of pharmaceuticals on the environment and human health. and (Khan et al., 2020; Lonappan et al., 2016; Schwarzenbach et al., 2006).

In this work, DCF sodium and pCBA were chosen as model test pollutants and treated with two plasma sources with different reactor geometry under a variety of experimental conditions. DCF non-steroidal anti-inflammatory drug (NSAID) is used on a global scale to treat inflammatory diseases and reduce pain and fever (Rodrigues et al., 2021; Sathishkumar et al., 2020). According to the authors' statistics, a large amount of DCF, approximately >1000 tons, is used globally each year (Lonappan et al., 2016). As a consequence, DCF is regularly observed in high concentrations in sewage treatment plant effluents that are persistent enough to be found in surface, ground and even drinking water. and (Heberer and Feldmann, 2005; Lonappan et al., 2016). The presence of DCF in water can play a toxic influence on aquatic life, plants and human health (Deng et al., 2021; Sathishkumar et al., 2020). This also led to the unprecedented decline of vultures in India (Taggart et al., 2009). Consumption of DCF has been banned by various countries (e.g. India, Nepal, Bangladesh, etc.) in order to reduce the further decline of the vulture population (Markandya et al., 2008). The pCBA was the second compound that was chosen for the treatment as it is used in various chemical syntheses. The pCBA was found as a by-product in the treatment of various organic chemicals (Bing et al., 2012). The pCBA is an industrial chemical that is commonly used in the pharmaceutical industry. Since it has strong reactivity with HO•, pCBA was also utilized as a probe compound in several water treatment procedures to determine HO• levels (Bing et al., 2012; Pi et al., 2005).

Since conventional wastewater treatment plants (WWTPs) do not completely decompose a large number of OMPs of anthropogenic origin due to unfavorable properties such as poor biodegradability, they are released into natural water bodies (Sathishkumar et al., 2020). For example, conventional WWTPs are reported to remove just 30–70 % of DCF from wastewater streams (Deng et al., 2021; Lonappan et al., 2016). As a result, untreated DCF effluents from WWTPs enters the environment and pollutes ecosystems. Previous research has also stated that DCF can interact with other organic molecules in the environment, leading to the production of other harmful contaminants (Mukherjee et al., 2022).

AOPs have been used successfully as a tertiary treatment method and are regarded as a promising method in the field of wastewater treatment to eliminate OMPs (pharmaceuticals, organic dyes, pesticides, etc.) (Cuerda-Correa et al., 2019; Garrido-Cardenas et al., 2020). The primary feature of AOPs is the generation of HO• radicals (high oxidizing potential), which are particularly reactive with a wide variety of organic contaminants and then degrade them, resulting in effective mineralization of organic pollutants into H_2O and CO_2 (An et al., 2010; Wang and Xu, 2012). The goal of generating HO• radicals, different AOPs based on chemical admixture (O_3/H_2O_2, O_3/UV, O_3/UV/H_2O_2), photocatalysis (UV/TiO_2, UV/TiO_2/H_2O_2), Fenton (Fe_2^+/H_2O_2, Fe_2^+/UV/H_2O_2) and application of electric energy (electrochemical oxidation: Anodic, Electro-Fenton) have been addressed and shown in past study (Amor et al., 2019; Kumar et al., 2021; Macías-Quiroga et al., 2021; Wang and Xu, 2012). The majority of AOPs rely on external chemicals and catalysts to create HO• radicals. There are some reviews where authors revealed possible possibilities and limitations related with various AOPs for OMPs degradation (Hijosa-Valsero et al., 2014; Ma et al., 2021).

Cold atmospheric plasmas have been shown to effectively decompose OMPs effectively and are a promising innovative AOP that has been explored for water decontamination (Hijosa-Valsero et al., 2014; Kumar et al., 2022; Li et al., 2014; Magureanu et al., 2015; Malik, 2010; Topolovec et al., 2022). Gaseous plasma can be a very complex mixture of electrons, ions, metastables, UV lights, electromagnetic fields, electric fields, etc. (Bruggeman and Brandenburg, 2013; Chen, 2016; Foster, 2017; Jaiswal et al., 2020). The interaction of cold plasma with an open or controlled environment can produce a plethora of reactive species that can be used for a variety of beneficial chemical reactions in applications such as agriculture, medicine, sterilization, disinfection, material synthesis, electronics and so on (Barjasteh et al., 2021; Domonkos et al., 2021; Fridman, 2008; Tomić et al., 2021).

Plasma-liquid interactions have grown in popularity in recent years due to crucial characteristics such as the simultaneous production of many powerful chemical reactive oxidants at low temperatures, which has the ability to have a large impact on a variety of prospective applications. For example, the APPJ source which was used in this study for plasma formation in the gas phase above the liquid surface can cause a variety of chemical and physical effects, including the generation of reactive oxygen and nitrogen species (RONS: HO•, O•, HO_2, H_2O_2, O_3, NO_3^-, NO_2^-, NO•, $ONOO^-$, etc.), UV photons, as well as hydrated electrons (free electrons in the solution) without the usage of chemical agents (Bradu et al., 2020; Bruggeman et al., 2016; Foster et al., 2012; Lukes et al., 2014). The APPJ has a high potential for transporting highly concentrated reactive species from the gas phase to the liquid phase via the jet's gas flow (Bruggeman et al., 2016; Du et al., 2018). As a consequence, such a plasma source can be used as a green approach of destroying complex non-biodegradable organic contaminants. Previous studies attempted to use certain CAPs with various reactor configurations, powered by different electrical signals (AC, DC, RF sources), different working gases (argon, helium, oxygen, nitrogen) and several process parameters to decontaminate water (Hijosa-Valsero et al., 2014; Kumar et al., 2021; Malik, 2010). It was also noted that there have been a few earlier experiments that used CAPs to generate large plasma and surface contacts to remove organic contaminants from water.

The purpose of this study was to investigate the degradation of pCBA and DCF in aqueous solutions utilizing CAPs (pin-APPJ and multi-needle electrodes-APPJ with recirculation), as well as to compare the performance of both plasma reactors in terms of pollutants removal and energy yield. The pin-APPJ, which has 1 jet, was utilized to treat 5 mL of polluted water. The multi-needle electrodes-APPJ, which have 3 jets and continuous

recirculation, were utilized to treat a quarter liter of contaminated water. The approach of increasing the number of jets aims to increase the mass transfer of reactive species and consequently the kinetics of pollutant breakdown in water. The continuous recirculation approach improves the mixing of reactive species in the liquid and hence increases reactivity. The plasma source with multi-needle electrodes can lead to an easily scalable plasma source for treatment of large volumes of contaminated water. The efficient application of plasma pin-APPJs to the flowing contaminated sample, with large plasma/liquid surface area ratio, brings an advantage compared to large area Dielectric Barrier Discharge plasmas that are more complicated to sustain.

In this paper, we will present electrical characterization, Optical Emission Spectroscopy and ICCD (Intensified Charged Coupled Device) imaging of 1-pin APPJ and 3-pin APPJ. The measurements were made during the removal of pollutants from contaminated water samples. These two plasma devices are used for DCF and pCBA removal. The HPLC analytical instrument was used to study the degradation kinetics of DCF and pCBA. The obtained data was used to determine the energy yield and compared to the literature. The oxidation transformation products generated during the degradation of the DCF were detected using Orbitrap-LC-MS and possible degradation mechanisms were proposed.

2. Materials and methods

2.1. Experimental setup

Two plasma sources are used for the treatment of DCF and pCBA-containing aqueous solutions. The reactor geometry and the instrumental devices that were used are described in the following section.

2.1.1. Pin-electrode-APPJ

The schematic of the experimental setup of pin-APPJ and the picture of the plasma jet contacting the liquid sample is shown in Fig. 1a. The plasma source consists of a concentrically placed glass tube, a ceramic tube and a stainless steel wire as an electrode. The outer and inner diameters of the glass tube are 6 mm and 4 mm, respectively. The stainless steel wire with

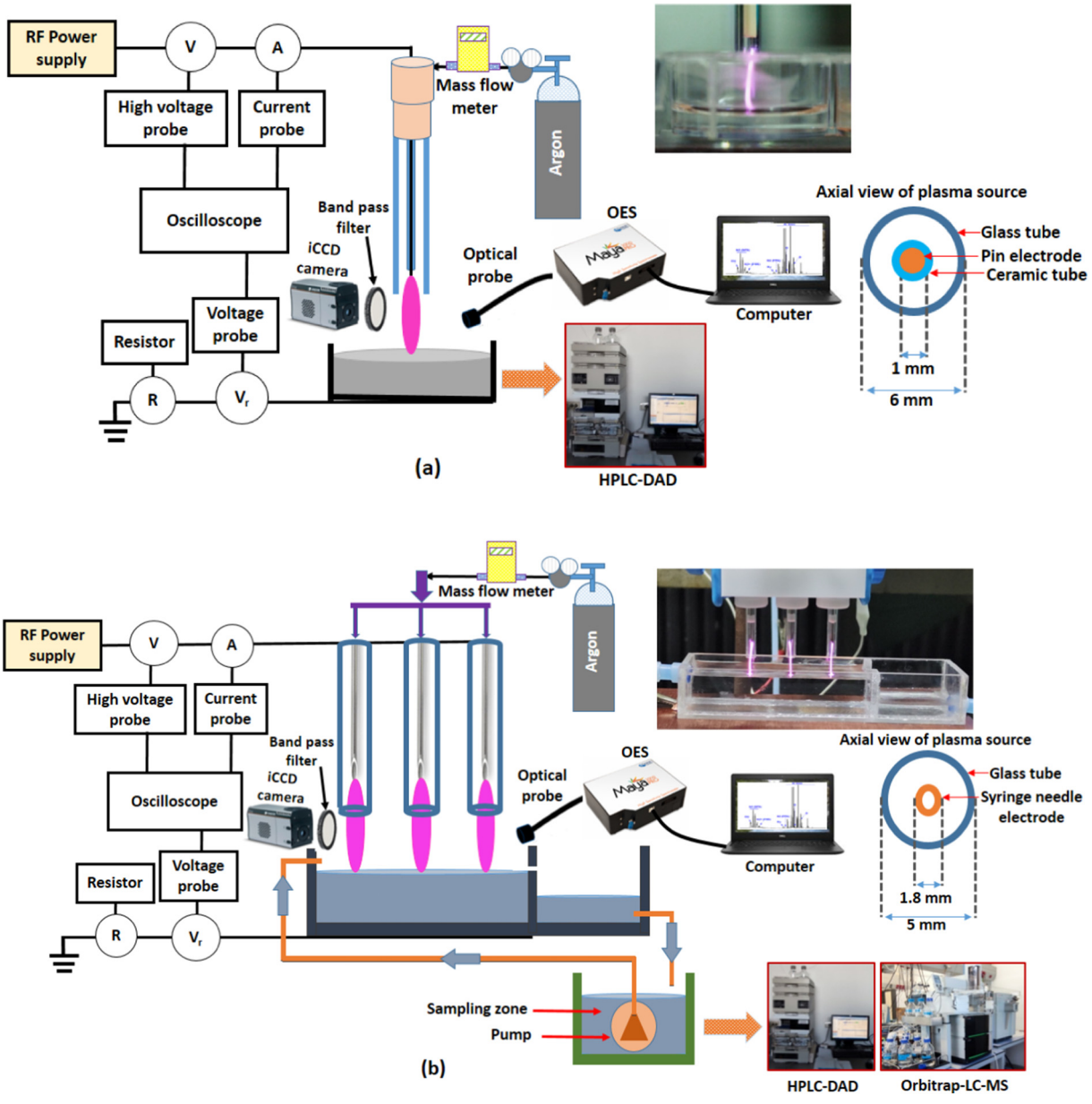

Fig. 1. The schematic diagram of experimental, (a) setup-pin-APPJ (left) with an image of plasma solution treatment (upper right), (b) multi-needle electrodes-APPJ with continuous flow treatment system (left) with plasma solution treatment (right).

a diameter of 1 mm with a sharpened tip is used as a high-voltage electrode and while the rest of the wire was covered with a ceramic tube. The electrode is powered by a high voltage radio frequency (RF) power supply with a frequency of 332 kHz. The other grounded electrode is the solution placed in a vessel with copper tape glued to the outer bottom side of the vessel and connected to the ground. In this configuration, plasma was generated between the electrode tip and stagnant liquid surface using argon as a working gas.

2.1.2. Multi-needle electrodes-APPJ

The schematic diagram of the experimental setup of multi-needle electrodes-APPJ is shown in Fig. 1b. The atmospheric pressure plasma jet over the flowing liquid surface was generated through a multi-syringe needle electrode type configuration. The inner and outer diameter of each needle was about 1 mm and 1.8 mm, respectively. The needles were inserted inside the glass tubes, where the inner diameter, outer diameter and length of each tube were about 3.7, 5 and 45 mm, respectively. The distance between the tip of each needle and the end of each tube was 7 mm. The distance between the two adjacent needle electrodes was 20 mm. The distance between needle tips and solution was set at 15 mm. Similarly as for a single-pin system, the copper tape was wrapped over the bottom of the sample vessel while the electrodes were supplied by a sine signal at a frequency of 351 kHz. Since the same power supply was used for the pin-electrode jet, the difference in the electrical impedance of the circuit causes a change in the signal frequency. Argon gas with a total flow rate of 2 slm (standard liter per minute) was used as a feed gas, distributed evenly between 3 pin electrodes.

In both configurations, the voltage (v) at the powered electrode was determined by a high voltage probe (Tektronix 6015A). The current at the powered electrode was measured with a current probe (Agilent N2783B). The voltage drop (v_r) across the 1 kΩ resistor used to establish the current in the grounded part (i_g) was recorded using a voltage probe (Agilent 10073C). The time variable voltage and current signals were monitored by using a 4-channel, 200 MHz, 2.5 GSPS digital oscilloscope (Tektronix MDO3024). Simultaneously, the data from the oscilloscope was transferred to a laptop for further analysis. The power delivered from the power supply to the plasma source and the power in the grounded line, i.e. the power deposited from the plasma passing through the sample, was calculated.

2.2. Treatment of solution

In the configuration of pin-electrode APPJ, 5 mL of solution was exposed to the jet with different treatment times. In each experiment, 2 mL of plasma-treated samples were taken for further analysis. In the assembly of the flow system, a total volume of 250 mL of solution was treated, where around 12 % of the solution was continuously exposed to the treatment zone. The solution was circulated by a pump (kept inside the solution reservoir) at a flow rate of 300 mL/min and a corresponding Reynolds number of 1349. The Reynolds number determines the flow pattern, hence at this value, the flow was in the laminar flow regime (Xiong et al., 2012). The total treatment times were 30 min for DCF and 50 min for pCBA, where 2 mL of samples were taken at specific intervals for analysis. In the event of the treatment of 5 mL using pin-APPJ (1 jet), each sample corresponded to a single experiment. In the case of treatment using a plasma (3 jets) recirculation system (volume 250 mL), there was continuous sampling at various time intervals.

In both experimental systems, there were minor reductions in volume due to heating and gas flow (always <0.4 % for 3 jets and 36 % for 1 jet, longer treatment time). The volume reduction was always recorded and incorporated into the final calculation of degradation removal. It shall also be noted that volatilization of the target contaminants is not expected due to their low volatility.

2.3. Solution characterization

DCF (chemical formula: $C_{14}H_{10}C_{l2}NNaO_2$, molecular weight: 318.13 g/mol, purity ≥ 98 %, CAS number: 15307–79-6) and pCBA (chemical formula: $C_7H_5ClO_2$, molecular weight: 156.57 g/mol, purity ≥ 98 %, CAS number: 74–11-3) were purchased from Sigma Aldrich.

In this investigation, DCF with initial concentrations of 25 mg/L and 50 mg/L and pCBA with initial concentrations of 25 mg/L and 40 mg/L were used in the treatment. First, a stock solution with a high initial concentration was prepared by dissolving each compound in distilled water. The lower concentration was obtained by diluting the concentrated solution with distilled water. Both DCF and pCBA are soluble in water to a considerable extent. For example, DCF and pCBA solubility in distilled water have been reported to be 2425 mg/L (Jankunaite et al., 2017) and 80 mg/L (Phatak and Gaikar, 1996), respectively. The initial concentrations chosen are greater than those found in the water bodies (ng/L to g/L). The higher initial concentrations evaluated allowed for proper examination of the degradation pattern. The authors claimed that prior studies on the degradation of OMPs by AOPs were also conducted in similar, higher initial concentration ranges (Kumar et al., 2021; Lesage et al., 2013; Rong et al., 2014).

Chromatographic analysis of the samples was carried out on an Agilent HPLC instrument, series 1100 (Agilent Technologies, Waldronn, Germany), with a photodiode array detector, using Hypersil BDS-C18 column (125 × 2 mm) with 5 μm particle size (Phenomenex, Torrance, USA), thermostated at 30 °C. All samples were filtered through a 0.2 μm cellulose filters (Agilent technologies, Santa Clara, CA, USA) prior to analysis. The mobile phase consisted of a 1 % (*v*/*v*) solution of orthophosphoric acid in ultrapure water (solvent A) and acetonitrile (solvent B). Acetonitrile and orthophosphoric acid were LC-MS grade (Fisher Scientific, Leics, UK) and ultra-pure water was generated by using the Water Purification System (New Human Power I Integrate, Human Corporation, Seoul, Republic of Korea). The flow rate of the mobile phase was 0.5 mL/min and the injection volume was 10 μL. A gradient program was used as follows: 80–30 % A, 0–7 min; 30–80 % A, 7–12 min (DCF) and 80–60 % A, 0–8 min; 60–80 % A, 8–12 min (pCBA). The detection wavelengths were set at 240 nm and 276 nm for pCBA and DCF, respectively. Quantification was performed using standardized calibration curves. The content of products in the samples was determined by calculation of peak area and expressed as milligrams per liter. Chromatographic data were recorded and processed by using HP ChemStation Chromatographic Software (Palo Alto, CA, USA).

The byproducts derived from the degradation of DCF were analyzed by using Orbitrap Exploris 120 high-resolution LC-MS (Thermo Fisher Scientific). A reverse-phase column (Hypersil GOLD-Selectivity C18, 3 μm, 2.1 mm × 50 mm) was used for the separation of the component in the mixture. The column temperature was set at 30 °C. The injection volume and flow rate was 10 μL and 0.4 mL/min, respectively. The analysis was carried out in a negative ion and positive ion mode with ionization voltages of 2500 V and 3500 V, respectively. Heated electrospray ionization (H-ESI) system was used as an ion source. The mass spectra were acquired in full scan mode in the mass range of 40 to 5000. In the positive ion mode, the mobile phase composition was HPLC water with 0.1 % formic acid and methanol. In the negative mode, the mobile phase consists of HPLC water with 5 mM ammonium acetate (at pH 8) and methanol. Variation in composition, first started with 98:2 % and increased up to 2:98 % in 4.7 min and remained constant for 6 min and decreased up to 98:2 % in 9 min. The extracted data was transferred to Thermo Scientific™ Compound Discoverer software for further processing. The software also provided an excel based report containing details of the compound, isotopes, retention time, mass to charge ratio, fragment ion, intensity, mass error (ppm), etc. The chemical structure and fragmentation pattern for each possible transformation product were drawn by using ChemSketch software (ACD/ChemSketch Freeware).

DCF and pCBA removal efficiency was defined as Eq. (1).

$$Removal\ (\%) = \frac{C_o - C \times d}{C_o} \times 100 \quad (1)$$

where C_0 (mg/L) is the initial concentration before plasma treatment, C (mg/L) is the final concentration after plasma treatment and d is the evaporation coefficient.

The energy yield of the removal of DCF and pCBA is determined by the following Eq. (2).

$$Energy\ yield\left(\frac{mg}{kWh}\right) = \frac{C_o\left(\frac{mg}{L}\right) \times V_o(L) \times \frac{1}{100} \times Removal(\%)}{P_{mean}\ at\ the\ sample\ (kW) \times t(h)} \quad (2)$$

where C_0 (mg/L) is initial concentration of the plasma treated compound, V_0 (L) indicates the initial volume of plasma treated compound, P_{mean} (kW) is discharge power at the sample and t (h) is the treatment time.

In all plasma treatment processes, the solution pH was determined by a pH meter (HANNA-HI1330).

2.4. Optical characterization

Plasma emission spectra was captured by using Maya2000 Pro-UV-NIR (Ocean Insight-High Sensitive Spectrometer) with an optical resolution of 0.18 nm full width at half maximum. The optical fiber (M114L02) length of 2 m and core diameter of 600 μm was placed perpendicular to the plasma jet in order to capture the emission from the whole volume of the plasma jet. The emission was recorded with an exposure time of 50 ms. The raw OES data was transferred to a laptop and analyzed in OriginPro data analysis software. Plasma emission is measured with and without plasma (background). The background spectra were subtracted from the plasma emission spectra to achieve the exact spectrum. The spectral intensity was corrected for the optical system efficiency.

The plasma emission profiles were characterized by using an Andor iStar DH734I ICCD camera with a Nikon UV-105 mm f/4.5 lens mounted. The lens of the ICCD camera was set perpendicular and in front of the plasma jet. During the analysis, the sample was filled in a quartz-type petri dish (to avoid the blockage of light having a lower wavelength (e.g. UV)) and placed under APPJ. There was no sample flow during ICCD imaging. In order to capture the spatial emission distribution of various reactive species (HO•, O•, H•, N_2 (SPS: second positive system & FNS: First negative system), Ar*), band bass filters (attached with holder) were used and placed in the front of the lens. The transmittance percentage of each filter was calculated by spectrophotometer (Beckman Coulter DU 720 UV/Visible). A MATLAB script was used to estimate the geometry of the plasma jet and to process ICCD camera images.

3. Results and discussions

3.1. Electrical measurements

The electrical measurements were implemented to investigate the discharge parameters (voltage, current, power deposition). The discharge voltage and current are the critical parameters that are used to obtain dissipated power in the plasma system. The high voltage was applied to the electrodes (to pin and multi-needles). The sharp edge electrode configuration was selected because it creates a high electric field around the tip. When the applied voltage is strong enough this electric field is enough for the breakdown to occur followed by the production of a conduction channel in the discharge gap.

The voltage-current parameters were investigated and the power deposition to the plasma system for both plasma sources was estimated. Fig. 2 displays the relationship between RMS voltage vs RMS current and power deposition at sample vs RMS voltage for 3-jets.

The mean power deposition at the sample was calculated using eq. 3, by averaging the instantaneous power (product of time-varying voltage $v(t)$ and time-varying current $i(t)$ waveforms) over a time interval of $n = 6$ periods.

$$P_{mean\ at\ sample} = \frac{1}{nT}\int_{T1}^{T2} v(t) \times i_g(t) \times dt \quad (3)$$

where, $P_{mean\ at\ sample}$: mean power at the sample; $v_R(t)$: voltage drop at the resistor; resistance $R = 1$ kΩ; $i_g(t)$: current at the ground (sample): $nT = T_2 - T_1$.

$$i_g\ (t) = v_R(t)/R \quad (4)$$

The plasma system was electrically described in two modes: when the plasma was ignited and when it was not. When there was no plasma ignition, voltage and current changed linearly, but voltage decreased after plasma discharge began (Fig. 2a). The power delivered to the sample after plasma ignition, which is essential in our investigation, was in the range of 5.8 W–16 W (Fig. 2b).

3.2. Optical characterization of plasma

3.2.1. OES measurements

The recorded spectra during the treatment of DCF by a multi-needle electrodes-flow system, shown in Fig. 3. The spectra between 200 and 427 nm, mainly correspond to various emission bands, such as the vibrational transition of HO• ($A^2\Sigma^+ \rightarrow X^2\pi$), N_2 SPS ($C^3\pi_u \rightarrow B^3\pi_g$), N_2^+ FNS ($B^2\Sigma_u \rightarrow X^2\Sigma_g$) and nitric oxide NO_γ ($A^2\Sigma^+ \rightarrow X^2\pi$). The spectrum lines between 697 and 965 nm are dominated by the excited argon atoms (4p → 4 s) and O• ($3p^5P \rightarrow 3s^5S$ and $3p^3P \rightarrow 3s^3S$). The spectra of N_2 SPS, N_2^+ FNS, O• and NO_γ are typical for open-air-argon plasma discharges operating above a water sample (Lamichhane et al., 2022).

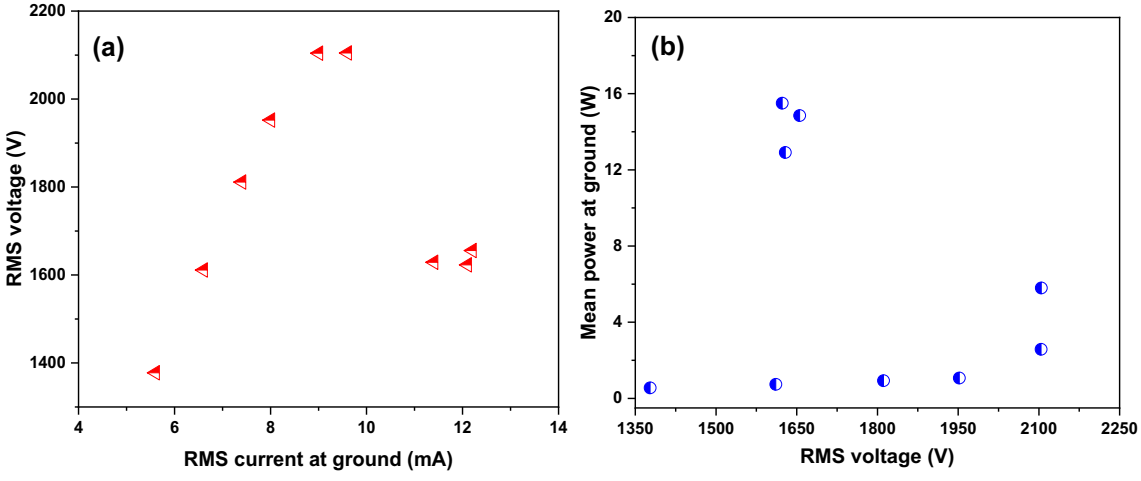

Fig. 2. (a) V-A characteristics (RMS voltage as a function of RMS current at sample/ground), (b) variation of mean power (delivered at the sample/ground) as a function of RMS voltage.

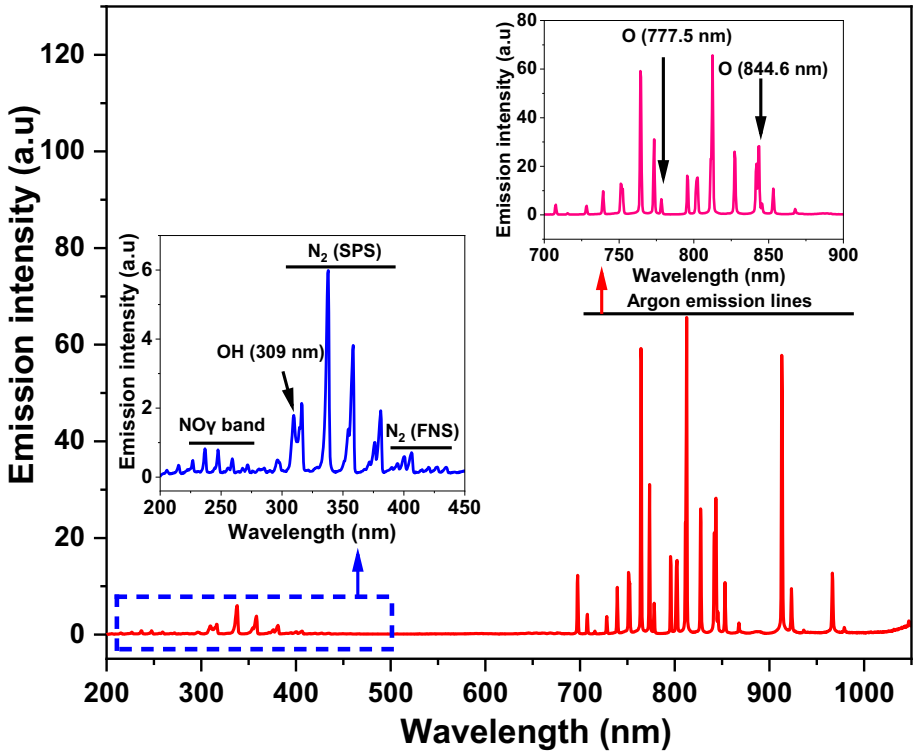

Fig. 3. The emission spectrum of argon – atmospheric pressure plasma jet in contact with ambient air and over the liquid surface, integration time 50 ms. Experimental conditions: C_0 = 25 mg/L (DCF), V_0 = 250 mL, P_{mean} at the sample 8 W, argon flow of 2 slm. Inset graphs depict the zoomed-in portion.

The collision of energetic species with H_2O molecules may be the primary source of HO• production (Eqs. (5) & (6)) (Invernizzi et al., 2020; Jaiswal and Aguirre, 2021). Water molecules in the gas phase are formed mainly through evaporation, plasma species bombardment, gas movement and air (Ghimire et al., 2021; Liu et al., 2016). The threshold energy required to dissociate H_2O by electron impact dissociation is approximately 4.4 eV. As a result, the reaction necessitates a lower electron temperature, which is easily attained in argon-APPJ.

$$e^- + Ar \rightarrow Ar^* + e^- \quad (5)$$

$$e^- + H_2O \rightarrow HO^{\cdot} + H^{\cdot} + e^- \quad (6)$$

In general, argon metastables have energies ranging from 11.5 to 11.8 eV, which is high enough to react with H_2O as well as excite N_2 ($C^3\pi_u \rightarrow B^3\pi_g$, 11.03 eV) (Soler-Arango et al., 2018), as explained by the following reactions (7) and (8).

$$Ar^* + H_2O \rightarrow HO^{\cdot} + H^{\cdot} + Ar^* \quad (7)$$

$$Ar^* + N_2 \rightarrow N_2^* + Ar \quad (8)$$

Excited molecular nitrogen and its metastables have enough energy to react with and dissociate H_2O molecules (Eq. (9)) (Adhikari et al., 2021; Uhm et al., 2018).

$$N_2^* + H_2O \rightarrow HO^{\cdot} + H^{\cdot} + N_2 \quad (9)$$

The threshold energy for N_2^+ ion generation is substantially greater (18.8 eV) than for excitation, hence the FNS band appeared with much lower intensity (Cullen and Milosavljević, 2015; Gazeli et al., 2015). One possibility for the FNS generation reaction is that argon metastables with high energy can ionize N_2 via impact excitation and ionization (Eq. (10)).

$$Ar^* + N_2 \rightarrow N_2^+ + Ar + e^- \quad (10)$$

Atomic O can originate after the dissociation of molecular O_2 by energetic electrons and argon metastables via collisional dissociation (Eqs. (11) & (12)). The process reaction requires lower threshold energy (below 11 eV) (Adhikari et al., 2021).

$$Ar^* + O_2 \rightarrow O^{\cdot} + O^{\cdot} + Ar \quad (11)$$

$$e^- + O_2 \rightarrow O^{\cdot} + O^{\cdot} + e^- \quad (12)$$

The emission from the NO_γ system was observed. NO_γ production is caused by admixing air within the plasma (Yousfi et al., 2011), described by the following equations.

$$N^{\cdot} + HO^{\cdot} \rightarrow {}^{\cdot}NO + H^{\cdot} \quad (13)$$

$$O^{\cdot} + N^{\cdot} \rightarrow {}^{\cdot}NO \quad (14)$$

The presence of UV emission in the APPJ can also generate strong oxidants, such as HO• and O• by photolysis of H_2O and O_2 (Attri et al., 2015; Invernizzi et al., 2020).

From the point of water decontamination, the presence of HO• and O• in the plasma is found to be major short-lived oxidants having high oxidative potential that can break down almost most non-biodegradable refractory organic substances by the following reaction mechanism: hydrogen atom abstraction, electrophilic addition and electron transfer reactions. Abundant excited argon and other RONS can also play an important role in water decontamination (García et al., 2017; Yehia et al., 2020). The reactive species produced by the plasma-gas-liquid-interface can transfer/diffuse/penetrate in the liquid phase and form secondary reactive species in the bulk solution, which can further drive degradation and change the pH and conductivity of the solution (Bruggeman et al., 2016; Foster et al., 2012; Kumar et al., 2022; Lukes et al., 2014).

We have also performed OES for pin-APPJ, which can be found in our prior published work (Kumar et al., 2022) and it was found that the emission spectra were almost identical. In case of pin-APPJ, a weak H_α line

was present in the spectra, but the H_α emission line was absent in multi-needle electrodes-APPJ, which might be created and promptly quenched.

The production of RONS in liquid phase is directly connected to the plasma chemistry in gas phase and gas/liquid interface (Bruggeman et al., 2016; Lukes et al., 2012; Pawłat et al., 2019). The presence of reactive species in the gaseous phase of plasma discharge responsible for further reactions at plasma gas/liquid interface can be determined by OES. In our previous work, we have used several methods for the quantification of long lived RONS in the plasma treated liquid (Kumar et al., 2022; Tomić et al., 2021). Several long-lived RONS (e.g., H_2O_2, NO_3^- and NO_2^-) were detected and quantified in the aqueous phase.

3.2.2. ICCD imaging of pin and multi-needle electrodes-APPJ

3.2.2.1. ICCD imaging of pin-APPJ. The ICCD imaging with filters was performed to investigate the spatial resolution emission of reactive species produced by argon-APPJ when it interacts with liquid in the presence of ambient air. Various optical filters (310 nm, 425 nm, 660 nm and 780 nm) were employed to identify certain lines/bands inside the plasma. Each filter's bandwidth (bandpass region) was around 10 nm. Acquisition parameters such as gate pulse width, exposure time and gain remained constant during ICCD imaging with filters. Fig. 4 shows the spatially resolved ICCD images.

The emission of HO• and vibrationally excited N_2 (SPS, 315.8 nm) was monitored using a filter with a center wavelength of 310 nm. The emission from mostly O• was measured at 777.5 nm in combination with excited argon (since excited argon also emits near 780 nm) using a 780 nm-centered filter. The filter with a central wavelength of 660 nm is primarily employed to record H_α emission at a wavelength of 656 nm. The emission of excited N_2 (SPS) and ionic nitrogen N_2^+ (FNS) was monitored using a 425 nm filter.

Fig. 4a shows an image captured using a 310 nm filter. Fig. 4b shows the images associated with the remaining filters, such as 780, 425 and 660 nm; the intensity level in these images was kept constant. In the case of the 310 nm filter, the emission from HO• (containing N_2 SPS) was extensively dispersed across the active plasma. It should be noted that the images with the highest emission intensity were obtained using 310 nm filters. The emission profiles recorded at 425 nm, 660 nm and 780 nm were nearly identical. Nevertheless, intense emission occurred in the case of the 780 nm filter (mainly owing to plasma interaction with the ambient air) and dominated at close to the liquid surface. Overall, ICCD time-integrated images demonstrated the presence of several reactive species in the plasma that could be responsible for the degradation of chosen OMPs in this investigation.

3.2.2.2. ICCD imaging of multi-needle electrodes-APPJ. The ICCD time-integrated imaging of multi-needle electrodes-APPJ was also done. The camera and filters were placed in such a way that they captured emissions from all three jets. Fig. 5 displays images captured with 310 nm and 780 nm filters, with the intensity scale constant for both filters for comparison. The spatially resolved emission intensity in all three jets was observed to fluctuate in both filters. For example, one jet's intensity was higher while the intensity in the other two jets was different at the same time. The variation in emission intensities could be related to a different level of excitation in the jets.

The emission intensity profile of HO• and N_2 (SPS) was brighter all along the jets but more intense in the middle jet, which could be owing to an intense concentrated electric field and excitation. O• and excited argon were observed in the jets, but strong emission was noticed in the middle of all three jets and the intensity was significantly reduced downstream at the jets' top.

3.3. Treatment of pharmaceuticals with pin-APPJ and multi-needle electrodes-APPJ

3.3.1. Pin-APPJ

The treatment studies were carried out by directly exposing the pin-APPJ to an aqueous solution containing DCF and PCBA while taking into account various experimental parameters that influence the degradation of both compounds. The parameters, such as initial pollutant concentration and treatment time, were adjusted and the resulting degradation results were thoroughly explained.

Fig. 6a depicts the degradation of pCBA in solution as a function of plasma treatment time. The degradation profile revealed that more than half of the initial pCBA concentration was eliminated in the first 5 min. The greatest degradation occurred in the first 3 min, with degradation efficiency values of approximately 63 % for 25 mg/L and 56 % for 40 mg/L. The initial concentration has a considerable impact on the behavior of the oxidation curves during the first 3 min of plasma treatment. After 10 min of treatment, both degradation curves merged, resulting in the complete removal of pCBA.

We fitted the data displayed in Fig. 6a to obtain pCBA degradation kinetics. The kinetics of pCBA decay demonstrate that it is well suited to the first order:

$$\ln \frac{C}{C_o} = -kt \tag{15}$$

where k is the kinetic rate constant.

The calculated R^2 (correlation coefficients) was evidence that the degradation of pCBA fitted well with first-order kinetics. Lower initial pCBA concentration promoted the highest degrading first-order rate constant, while larger initial pCBA concentrations reduced the rate constant. Higher concentration of pCBA represents more pCBA molecules in the

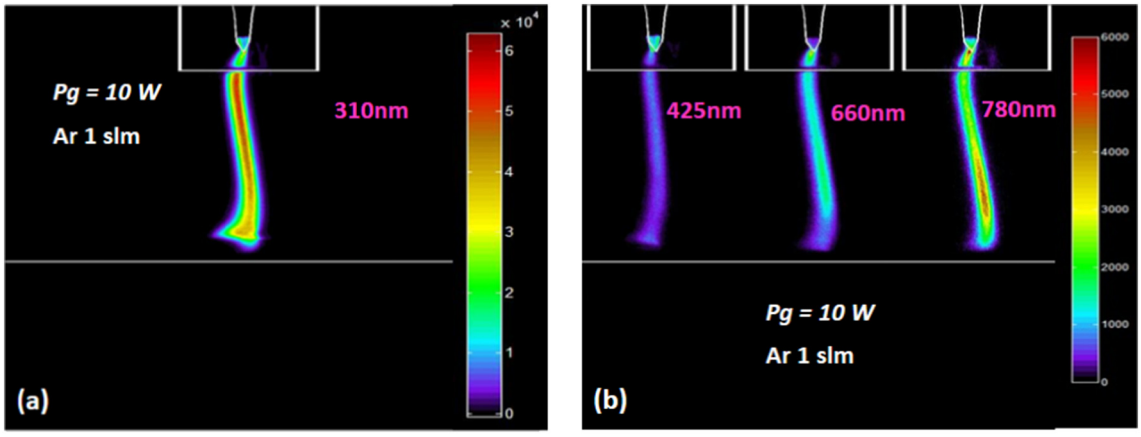

Fig. 4. The ICCD images with filters, (a) 310 nm, (b) 425 nm, 660 nm and 780 nm. Acquisition parameters: exposure time 20 ms, gate pulse width 5 ms and gain 50.

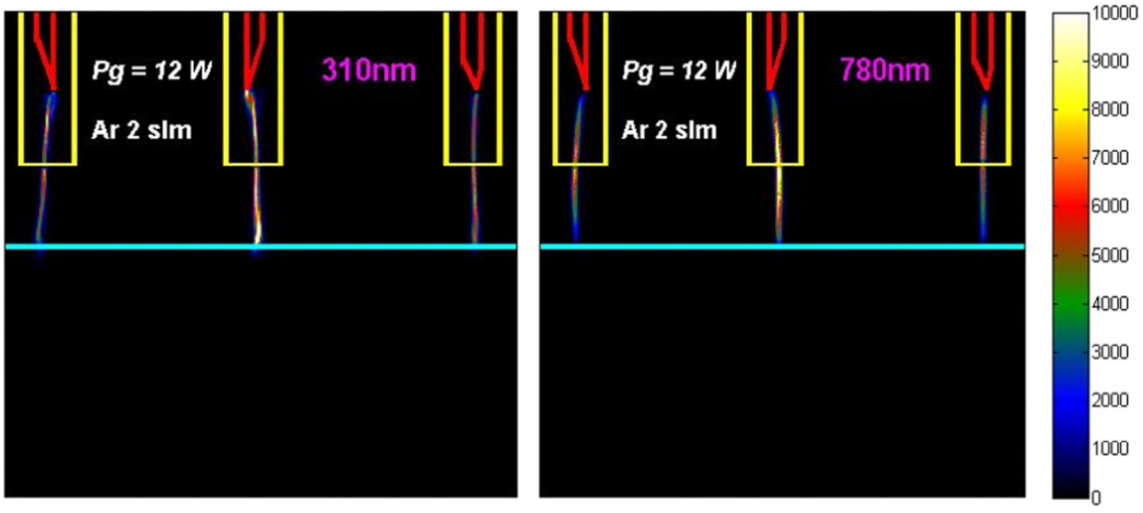

Fig. 5. The ICCD images with filters (310 nm and 780 nm). Acquisition parameters: exposure time 20 ms, gate pulse width 3 ms and gain 80.

solution resulting in more reaction sites for plasma species. Moreover, during the treatment by-products of pCBA are formed so not all introduced plasma species continue reacting with the original pCBA molecules. Taking into account that the rate of plasma species production remains relatively constant in time this can lead to lower degradation rate at higher concentrations.

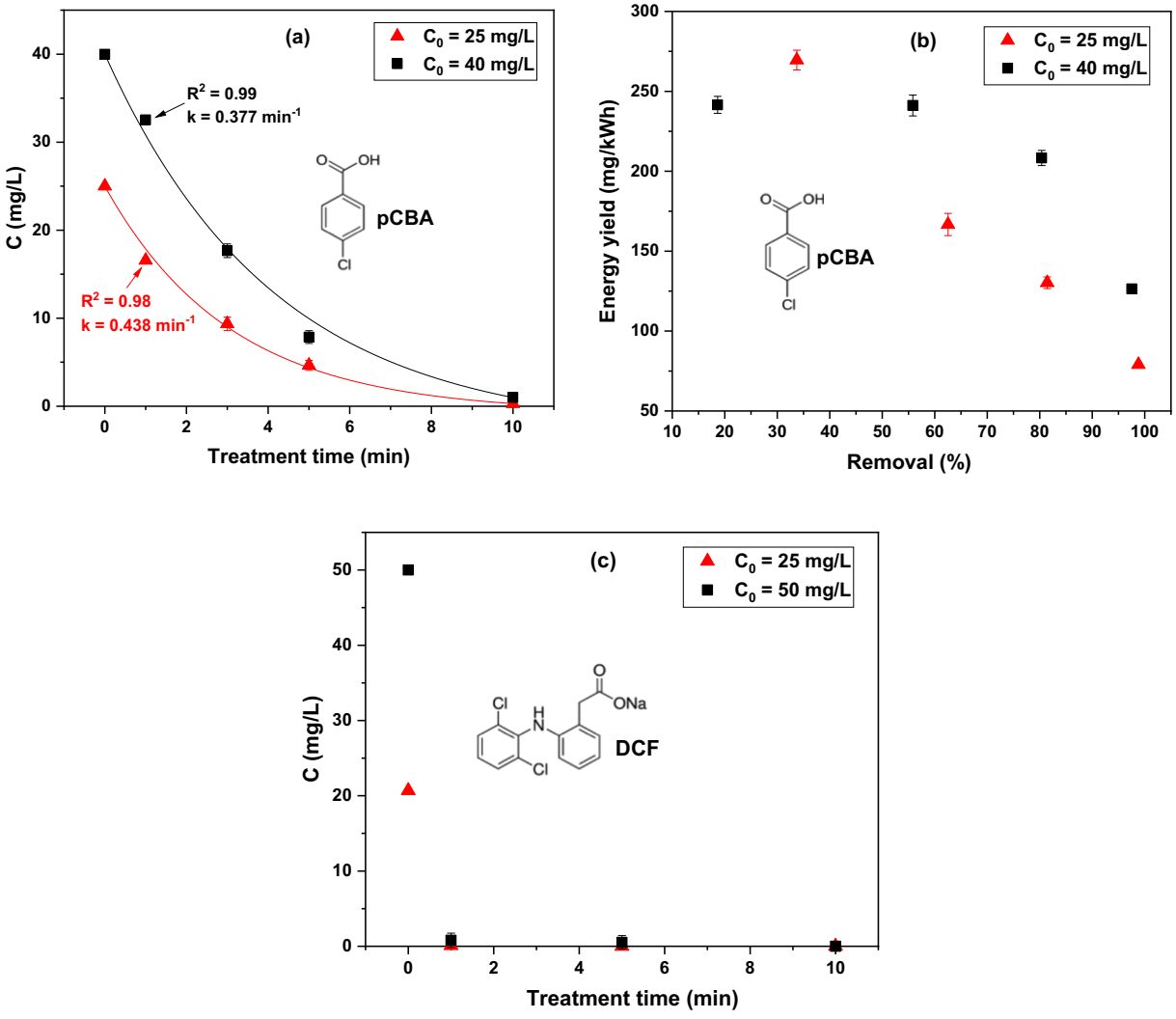

Fig. 6. (a) Change in pCBA concentration with treatment time, (b) energy yield vs removal %, (pCBA, C_0 = 25 mg/L and C_0 = 40 mg/L) and (c) change in DCF concentration with treatment time (DCF, C_0 = 25 mg/L and C_0 = 50 mg/L). Experimental conditions: V_0 = 5 mL, argon flow of 1 slm, P_{mean} at the sample 10 W.

Consequently, the half-life ($t_{1/2}$) pCBA decomposition time was determined as:

$$t_{1/2} = \frac{0.693}{k} \tag{16}$$

The time required to remove 50 % of the pCBA was 1.58 min for 25 mg/L and 1.83 min for 40 mg/L.

Aside from degradation, energy yield is a significant factor to consider in investigating the energy effectiveness of the plasma source. The energy yield for removing pCBA was calculated. Fig. 6b depicts the energy yield for removing pCBA as a function of removal %. Because of the longer treatment duration, the energy yield was lower at higher removal. For a longer treatment, power deposition may become increasingly concentrated in unproductive processes (e.g., the interaction of byproducts with plasma-induced species), resulting in a drop in energy yield. In the literature on plasma-based treatment, the energy yield is typically reported in terms of 50 % elimination for comparison. As a result, the amount of energy required to decompose 50 % of contaminants was calculated. Energy yield at 50 % pCBA elimination was 253 mg/kWh for 25 mg/L and 354 mg/kWh for 40 mg/L, respectively. More detailed comparison of the data on energy yield collected from the literature for pCBA removal by plasma was given at the end of Section 3.3.2.

DCF was treated with plasma while the same experimental conditions were considered as pCBA. As the solution was subjected to plasma, DCF decayed rapidly, as shown in Fig. 6c. The rapid degradation in the early stages of the process suggests that the majority of plasma-induced reactive species interacted and oxidized DCF. The chemical nature of organic substances (e.g. structural features/chemical reactivity) influences degradation. It has been found, for example, that DCF is strongly reactive not only with HO•, but also with other oxidants. As a result, HO• and other reactive species may play a significant role in the rapid degradation of DCF.

The degradation kinetics of DCF was not established because DCF practically vanished in 1 min and there were just a few points available to analyze the kinetic behavior. So, in our paper, we just reported the DCF degradation pattern.

The energy yield for DCF removal could not be determined precisely from the obtained measurements since DCF degraded quickly during the shortest sampling interval of 1 min for both initial concentrations. From these measurements, we can only conclude that the energy yield for DCF was higher than pCBA.

The pH of plasma-treated pCBA and DCF solutions was found to be lower after treatment. After 10 min of plasma treatment, the pH of pCBA decreased from 4 to 2.57 at 25 mg/L and to 2.65 at 40 mg/L. In the instance of DCF, the initial pH of the DCF solution was 6, but after 10 min of plasma treatment, the pH dropped to 2.66 at 25 mg/L and 2.69 at 50 mg/L. In both cases, the final pH was reduced to similar values after 10 min of plasma treatment. Additional experiments were conducted to treat distilled water without contamination with the same system of pin-APPJ. After 10 min of treatment, the pH of distilled water was reduced from 6.5 to 2.62. So, the reduction of pH is not related to contaminants but probably to plasma-induced nitrogen-based species. Changes in pH demonstrated the existence of acidogenic species (inorganic acids) in the liquid after plasma liquid interaction with ambient air (Judée et al., 2018; Rezaei et al., 2019). The authors found that the principal acidic species formed in the liquid are HNO_3 and HNO_2 (Thirumdas et al., 2018; Wenjuan and Xiangli, 2007). In water, these strong acids dissociate to their respective anion and a hydronium ion. Researchers determined that the pH value influences the degradation kinetics of OMPs in water -lower pH results in faster degradation. Rong et al., 2014, for example, investigated DCF degradation using an air DBD plasma source and reported that DCF removal was greater at pH 2.9 and 6.15 as compared to an alkaline environment at pH 10.1. Similar effect of low pH on pCBA degradation was reported in a study conducted by He et al., 2011. According to these results, we presume that lowering the pH value in the plasma treatment in our experiments contributed to the degradation of DCF and pCBA.

3.3.2. Multi-needle electrodes-APPJ

Another approach for treating significant amounts of polluted water, at least a quarter liter, was tested. Treatments were carried out using a continuous flow system with varying treatment times. The plasma source with multi-needle electrode geometry was employed to create plasma over the recirculated DCF and pCBA solutions. The goal of generating multi plasma jets over the recirculation solutions was to increase the plasma-liquid contact area and introduce more reactive species into the liquid, which can enhance the degradation.

The DCF degradation curve as a function of treatment time is depicted in Fig. 7a. DCF decayed significantly in the first 10 min at both initial DCF concentrations, although the rate of degradation was faster at the lower initial concentration. The complete removal of DCF was seen with both initial concentrations in 30 min. The quicker degradation could be explained by plasma-generated reactive components participating in DCF removal.

To undertake the kinetic analysis and determine the reaction order and rate constant, the experimental results were evaluated. When the treatment was performed at an initial concentration of 25 mg/L, the decay of DCF was well-matched with a first-order equation with a rate constant of 0.145 min^{-1}. The first order revealed that plasma-generated reactive species not only interacted with DCF, but also with intermediate products. DCF degradation is governed by a zero-order equation for rich initial concentrations, such as 50 mg/L and the rate of degradation was 1.636 mgL^{-1} min^{-1}, as indicated by provided Eq. (17). Zero-order decay (Eq. (17)) demonstrates that the reaction rate is steady and independent of DCF concentration.

$$C = C_0 - kt \tag{17}$$

The time required to degrade 50 % of DCF was assessed and the half-life ($t_{1/2}$) for zeroth-order decay was calculated using the given Eq. (18). It took roughly 5 min for lower initial concentrations of DCF to degrade 50 % and three times longer for higher concentrations.

$$t_{1/2} = \frac{C_0}{2k} \tag{18}$$

Fig. 7b depicts the calculated energy yield as a function of DCF removal for two initial concentrations. DCF concentration has a substantial impact on energy yield. The high energy yield for DCF elimination is most likely owing to a greater contribution of plasma-induced reactive species to the oxidation process. At 25 mg/L and 50 mg/L, the energy yield values were approximately 1542 mg/kWh and 3084 mg/kWh for complete degradation of DCF, respectively.

Multi-needle electrodes-APPJ was also explored for the treatment of pCBA, the degradation result can be seen in Fig. 7c. During the treatment of pCBA, slow degradation was observed, about 24 % removal of pCBA after 50 min of plasma treatment. A kinetic study was conducted to explore the kinetic behavior of pCBA. The investigation was carried out with only three treatment times in consideration. The degradation of pCBA corresponded closely to a first-order equation. The kinetic constant for pCBA was 0.00497 min^{-1}, which was lower than the kinetic constant for DCF.

The slow decomposition of pCBA in a case of 3-pin APPJ can be attributed to the different experimental setup compared to 1-pin APPJ. In case of 3-pin jet, although the effective plasma-liquid contact is larger than in case of 1-pin APPJ here we had a better mixing of the contaminated sample. This could lead to a higher competition for the reactive oxygen species (HO• radicals for example), which plays important role in interactions with pCBA byproducts and with the original compound. Also, increment of treated volume is reducing the efficiency of the treatment as with DCF compound.

The obtained energy yields at 50 % removal of DCF and pCBA by both plasma sources are estimated and compared to previous plasma-based DCF and pCBA removal. As previously stated, DCF was the most efficiently degraded pollutant in both plasma sources in our investigation. However, when the plasma sources were compared, the resulting energy yields were

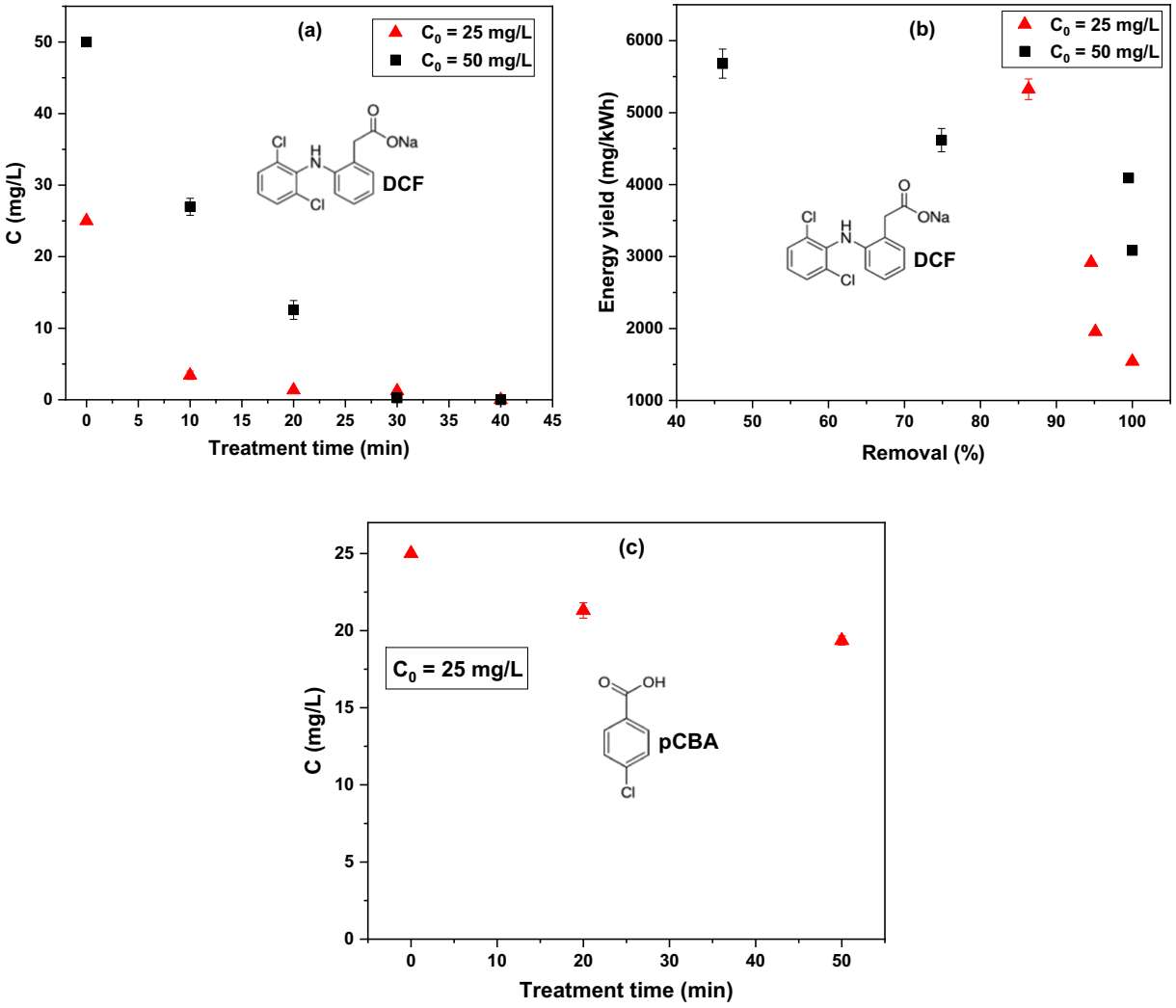

Fig. 7. (a) Change in DCF concentration with treatment time, (b) energy yield vs removal %, (DCF, C_0 = 25 mg/L and C_0 = 50 mg/L) and (c) change in pCBA concentration with treatment time (pCBA, C_0 = 25 mg/L). Experimental conditions: V_0 = 250 mL, argon flow of 2 slm, P_{mean} at the sample 8 W.

approximately one order of magnitude higher in multi-needle electrodes-APPJ than in pin-APPJ. This can be attributed to the increased plasma-liquid contact caused by three jets and a large initial volume, which results in a larger energy yield. In case of pCBA removal, the difference in energy output obtained with both plasma sources was not statistically significant.

Authors, for example, Dobrin et al., 2013 reported 1000 mg/kWh for 50 % and 760 mg/kWh for energy yield 90 % removal during the degradation of DCF by using pulsed corona discharge, where the plasma was formed over a liquid surface. Deng et al., 2021 used dielectric barrier discharge (DBD) plasma and obtained 2458 mg/kWh for 50 % and 1332 mg/kWh for 90 % DCF removal. According to Back et al., 2018, after the treatment of DCF with DBD, energy yield values varied from 20 to 715 mg/kWh for removal up to 90 %. When compared to our work, where DCF treatment was performed with the three jets-recirculation system, published data show relatively low DCF removal energy yield. In case of pCBA treatment, Lesage et al., 2014 explored the DBD-recirculation system and plasma was generated over the thin falling film, they found 624 mg/kWh of energy yield for 50 % removal. In the study of Schönekerl et al., 2020, degradation of pCBA was carried out with a plasma-multi electrodes system, as a result, 320 mg/kWh energy yield was obtained for 50 % removal. The reported energy yield associated with pCBA removal in the literature was not significantly different from our results.

If we look at the results, we can see that efficient removal of pollutants with a high energy yield suggests that treatment of some pollutants by plasma with recirculation could be considered a potential method for wastewater treatment and the technology can also be scaled up for large polluted water treatment.

3.3.3. Degradation products and mechanism of DCF

The use of full-scan ultra-high performance liquid chromatography coupled to Orbitrap MS (UHPLC-Orbitrap-MS) allows the identification of seven TPs (see supplementary, Table S1) during the plasma treatment (by plasma recirculation system): DCF-154 ($C_8H_{10}O_3$), DCF-166 ($C_8H_6O_4$), DCF-202 ($C_8H_{10}O_6$), DCF-241 ($C_{14}H_{11}NO_3$), DCF-259 ($C_{14}H_{10}ClNO_2$), DCF-277 ($C_{14}H_9Cl_2NO$) and DCF-308 ($C_{14}H_9Cl_2NO_3$). The TP analysis data was processed with Compound Discoverer software (Thermo Scientific). Elemental composition and double-bond equivalent (RDB) were selected. In all cases, possible elemental compositions for ions with a deviation of ±5 ppm of error were assigned (see supplementary, Fig. S1-S7). On the basis of the TPs identified, tentatively DCF degradation pathways were proposed (Fig. 8).

Due to APPJ-liquid-interactions, abundant ROS can be produced such as including hydroxyl radicals (HO·), hydrogen peroxide (H_2O_2), singlet oxygen ($^1O_2$) and ozone (O_3) (Cheng et al., 2020; Foster, 2017). Thereby, HO• radicals can cleave DCF in the aqueous solution, leading to the formation of TPs, which could be further degraded and mineralized (Deng et al., 2021; Dobrin et al., 2013; Liu et al., 2019). Fig. 8 shows different reactions mechanisms HO·-mediated such as hydroxylation, dechlorination,

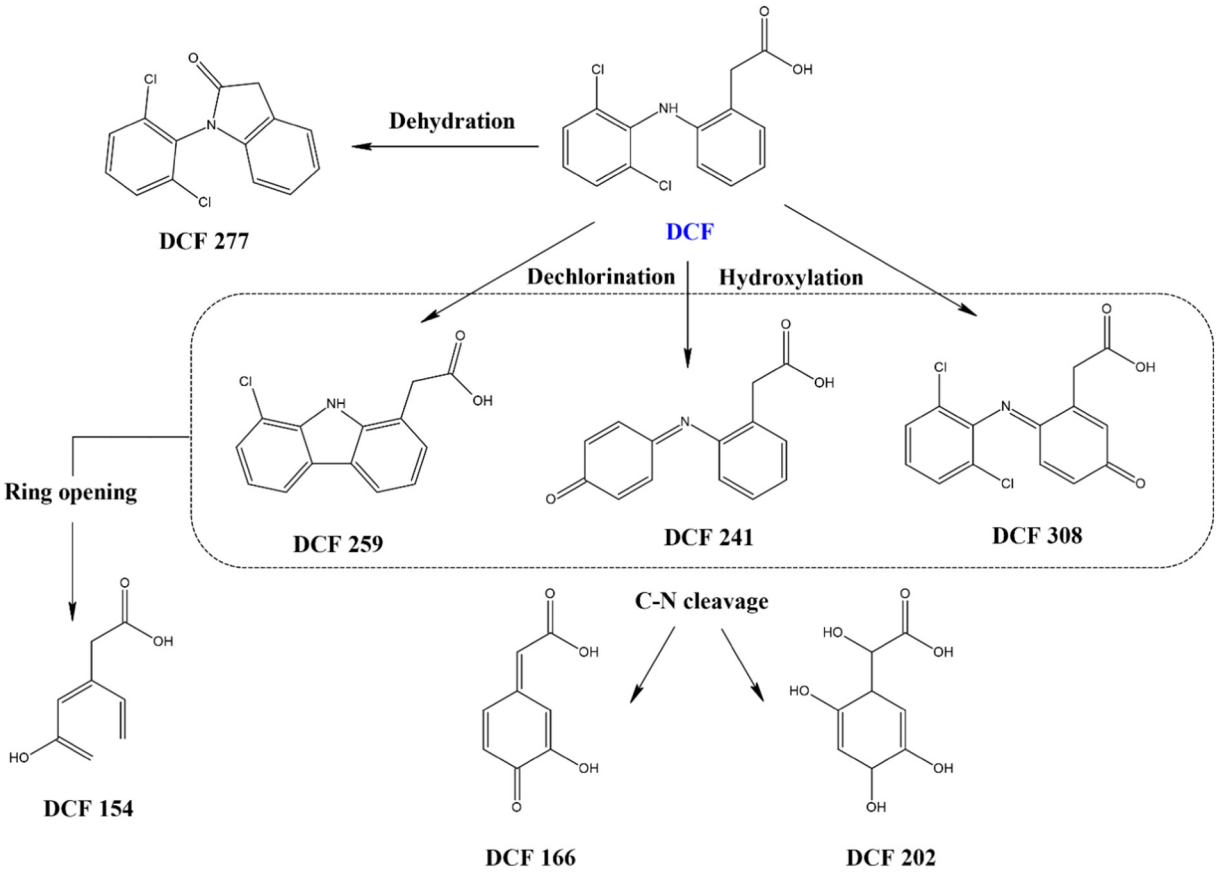

Fig. 8. Proposed possible reaction pathways for degradation of DCF.

cyclization and C—N cleavage, these tentative mechanisms are in agreement with the literature (Banaschik et al., 2018; Peng et al., 2021; Zhang et al., 2020).

The initial reaction of DCF with HO• to lead to either the abstraction of a hydrogen or the addition of the hydroxyl radical in the electron-donating position of the aromatic ring, DCF could undergo hydroxylation and lead to the production of $C_{14}H_{11}NO_3$ (DCF-241) and $C_{14}H_9Cl_2NO_3$ (DCF-308), it is known that HO· addition to benzene ring is kinetically more favored than H abstraction from the ring carbons (Agopcan Cinar et al., 2017). The presence of a Cl-benzyl bond in the aromatic ring of DCF resulted in fast dechlorination under plasma conditions and led to the release of chloride ions with reaction Gibbs free energies around 84–88 kcal/mol (Agopcan Cinar et al., 2017). Two dechlorination TPs were identified, $C_{14}H_{11}NO_3$ (DCF-241) and $C_{14}H_{10}ClNO_2$ (DCF-259). DCF-259 showed a transformation route involved the cyclisation into a carbazole derivative and loss of Cl (Salgado et al., 2013).

The mechanism suggested for the formation of DCF-277 ($C_{14}H_9Cl_2NO$) starts with cyclization and is followed by water elimination. According to Agopcan Cinar et al., 2017, nitrogen attack on the carbonyl carbon results in formation of the cyclic intermediate. DCF-277 was also identified in Sono-activated persulfate oxidation (Monteagudo et al., 2018).

Subsequently, the cleavage of C—N bonds could occur and form low molecular weight byproducts including $C_8H_{10}O_3$ (DCF-154), $C_8H_6O_4$ (DCF-166) and $C_8H_{10}O_6$ (DCF-202). The cleavage of the C—N bond can be facilitated by the attack of reactive species at the amino group in DCF and breaking the bridge of aromatic rings. Degradation of DCF could continue by cleavage of the ring and the formation of small molecules.

4. Conclusion

In this study pin-APPJ and multi-needle electrodes-APPJ sources were utilized as chemical free AOPs approaches for degradation of DCF and pCBA in water. We have constructed the 3-pin APPJ to be able to treat larger volumes and in flow regime. Both plasma sources operated in argon as a working gas and plasma was in contact with contaminated samples during the treatments. We have performed electrical characterization and obtained power deposited in the plasma in contact with liquid. This was necessary because power given by the power supply is not the same as power actually deposited in the discharges due to the losses in the system. The power deposited in the part of the discharge in contact with sample was needed for more precise calculation of energy yield. OES and ICCD imaging showed the presence and spatial distribution of excited species (for example HO•, O•, N_2 (SPS), argon excited species etc.) that are major initiators of the reactions in the liquid phase.

Pollutant degradation was efficient by using both plasma sources with DCF degrading much faster than pCBA. For both contaminants, the degradation was more efficient with 1-pin APPJ due to the much smaller volume of the contaminated sample. The results showed that the multi-needle electrodes-APPJ treatment was more energy-efficient and the energy yield varied by the magnitude difference. The maximum energy yield values at 50 % elimination were 6465 mg/kWh and 4036 mg/kWh for DCF concentrations of 25 mg/L and 50 mg/L, respectively. The energy yield for pCBA removal was much lower. With the introduction of recirculation of contaminant, plasma created RONS had more time to react. As a result, the plasma-recirculation system has the most substantial impact to the degradation process.

The elemental composition of transformation products of DCF was identified by high-resolution Orbitrap-LC-MS. The tentative molecular structure of transformation products was analyzed and compared to the literature. The DCF oxidation routes are described and products that formed after various reaction processes including hydroxylation, dechlorination and cyclization are reported based on the chemical formula and molecular weight.

Overall, the findings of this study indicate that cold plasma technology can be efficient option for removing organic pollutants from water that are

extremely difficult to degrade in conventional WWTPs. A multi-needle electrodes-APPJ recirculating system implemented in the research has the ability to enhance plasma and liquid interaction.

CRediT authorship contribution statement

Conceptualization A.K. N.P., W.G., N.S.; writing – original draft preparation A.K., review and editing A.K., N.S., N.P., W.G., O.J., A.P., S.Z., E.C.L., M.J.F; supervision N.P., W.G.; project administration N.P., W.G. All authors have read and agreed to publish the manuscript.

Data availability

Data will be made available on request.

Declaration of competing interest

The authors state that they have no known competing financial interests or personal ties that could have seemed to affect the work reported in this study.

Acknowledgments

This work was carried out under NOWELTIES project. NOWELTIES received funding from the European Union's Horizon 2020 research and innovation programme under the Marie Skłodowska-Curie grant agreement No. 812880. N.S., A.P., O. J. and N.P. are funded by the Ministry of Science, Techological Development and Innovation, grant number 451-03-68/2022-14/200024. This article is basedupon work from COST Action PlAgri, CA19110, supported by COST (European Cooperation in Science and Technology).

Appendix A. Supplementary data

Supplementary data to this article can be found online at https://doi.org/10.1016/j.scitotenv.2022.161194.

References

Adhikari, B.C., Lamichhane, P., Lim, J.S., Nguyen, L.N., Choi, E.H., 2021. Generation of reactive species by naturally sucked air in the ar plasma jet. Results in Physics 30, 104863. https://doi.org/10.1016/j.rinp.2021.104863.

Agopcan Cinar, S., Ziylan-Yavaş, A., Catak, S., Ince, N.H., Aviyente, V., 2017. Hydroxyl radical-mediated degradation of diclofenac revisited: a computational approach to assessment of reaction mechanisms and by-products. Environ. Sci. Pollut. Res. 24, 18458–18469. https://doi.org/10.1007/s11356-017-9482-7.

Amor, C., Marchão, L., Lucas, M.S., Peres, J.A., 2019. Application of advanced oxidation processes for the treatment of recalcitrant agro-industrial wastewater: a review. Water 11, 205. https://doi.org/10.3390/w11020205.

An, T., Yang, H., Li, G., Song, W., Cooper, W.J., Nie, X., 2010. Kinetics and mechanism of advanced oxidation processes (AOPs) in degradation of ciprofloxacin in water. Appl. Catal. B Environ. 94, 288–294. https://doi.org/10.1016/j.apcatb.2009.12.002.

Arslan, M., Ullah, I., Müller, J.A., Shahid, N., Afzal, M., 2017. Organic micropollutants in the environment: ecotoxicity potential and methods for remediation. Enhancing Cleanup of Environmental Pollutants. Springer International Publishing, Cham, pp. 65–99 https://doi.org/10.1007/978-3-319-55426-6_5.

Attri, P., Kim, Y.H., Park, D.H., Park, J.H., Hong, Y.J., Uhm, H.S., Kim, K.N., Fridman, A., Choi, E.H., 2015. Generation mechanism of hydroxyl radical species and its lifetime prediction during the plasma-initiated ultraviolet (UV) photolysis. Sci. Rep. 5, 1–8. https://doi.org/10.1038/srep09332.

Back, J.O., Obholzer, T., Winkler, K., Jabornig, S., Rupprich, M., 2018. Combining ultrafiltration and non-thermal plasma for low energy degradation of pharmaceuticals from conventionally treated wastewater. J. Environ. Chem. Eng. 6, 7377–7385. https://doi.org/10.1016/j.jece.2018.07.047.

Banaschik, R., Jablonowski, H., Bednarski, P.J., Kolb, J.F., 2018. Degradation and intermediates of diclofenac as instructive example for decomposition of recalcitrant pharmaceuticals by hydroxyl radicals generated with pulsed corona plasma in water. J. Hazard. Mater. 342, 651–660. https://doi.org/10.1016/j.jhazmat.2017.08.058.

Barjasteh, A., Dehghani, Z., Lamichhane, P., Kaushik, N., Choi, E.H., Kaushik, N.K., 2021. Recent Progress in applications of non-thermal plasma for water purification, biosterilization, and decontamination. Appl. Sci. 11, 3372. https://doi.org/10.3390/app11083372.

Bing, J., Li, L., Lan, B., Liao, G., Zeng, J., Zhang, Q., Li, X., 2012. Synthesis of cerium-doped MCM-41 for ozonation of p-chlorobenzoic acid in aqueous solution. Appl. Catal. B Environ. 115–116, 16–24. https://doi.org/10.1016/j.apcatb.2011.12.017.

Bradu, C., Kutasi, K., Magureanu, M., Puač, N., Živković, S., 2020. Reactive nitrogen species in plasma-activated water: generation, chemistry and application in agriculture. J. Phys. D. Appl. Phys. 53, 223001. https://doi.org/10.1088/1361-6463/ab795a.

Bruggeman, P., Brandenburg, R., 2013. Atmospheric pressure discharge filaments and microplasmas: physics, chemistry and diagnostics. J. Phys. D. Appl. Phys. 46, 464001. https://doi.org/10.1088/0022-3727/46/46/464001.

Bruggeman, P.J., Kushner, M.J., Locke, B.R., Gardeniers, J.G.E., Graham, W.G., Graves, D.B., Hofman-Caris, R.C.H.M., Maric, D., Reid, J.P., Ceriani, E., Fernandez Rivas, D., Foster, J.E., Garrick, S.C., Gorbanev, Y., Hamaguchi, S., Iza, F., Jablonowski, H., Klimova, E., Kolb, J., Krcma, F., Lukes, P., Machala, Z., Marinov, I., Mariotti, D., Mededovic Thagard, S., Minakata, D., Neyts, E.C., Pawlat, J., Petrovic, Z.L., Pflieger, R., Reuter, S., Schram, D.C., Schröter, S., Shiraiwa, M., Tarabová, B., Tsai, P.A., Verlet, J.R.R., von Woedtke, T., Wilson, K.R., Yasui, K., Zvereva, G., 2016. Plasma–liquid interactions: a review and roadmap. Plasma Sources Sci. Technol. 25, 053002. https://doi.org/10.1088/0963-0252/25/5/053002.

Chen, F.F., 2016. Introduction to plasma physics and controlled fusion. Third Edit. ed. Springer International Publishing, Cham https://doi.org/10.1007/978-3-319-22309-4.

Cheng, J.-H., Lv, X., Pan, Y., Sun, D.-W., 2020. Foodborne bacterial stress responses to exogenous reactive oxygen species (ROS) induced by cold plasma treatments. Trends Food Sci. Technol. 103, 239–247. https://doi.org/10.1016/j.tifs.2020.07.022.

Cuerda-Correa, E.M., Alexandre-Franco, M.F., Fernández-González, C., 2019. Advanced oxidation processes for the removal of antibiotics from waterAn Overview. Water 12, 102. https://doi.org/10.3390/w12010102.

Cullen, P.J., Milosavljević, V., 2015. Spectroscopic characterization of a radio-frequency argon plasma jet discharge in ambient air. Prog. Theor. Exp. Phys. 2015, 1–17. https://doi.org/10.1093/ptep/ptv070.

Deng, R., He, Q., Yang, D., Dong, Q., Wu, J., Yang, X., Chen, Y., 2021. Enhanced synergistic performance of nano-FeO-CeO2 composites for the degradation of diclofenac in DBD plasma. Chem. Eng. J. 406, 126884. https://doi.org/10.1016/j.cej.2020.126884.

Dobrin, D., Bradu, C., Magureanu, M., Mandache, N.B., Parvulescu, V.I., 2013. Degradation of diclofenac in water using a pulsed corona discharge. Chem. Eng. J. 234, 389–396. https://doi.org/10.1016/j.cej.2013.08.114.

Domonkos, M., Tichá, P., Trejbal, J., Demo, P., 2021. Applications of cold atmospheric pressure plasma technology in medicine, agriculture and food industry. Applied Sciences 11, 4809. https://doi.org/10.3390/app11114809.

Du, J., Liu, Z., Bai, C., Li, L., Zhao, Y., Wang, L., Pan, J., 2018. Concentration distributions and reaction pathways of species in the mass transfer process from atmospheric pressure plasma jet to water. Eur. Phys. J. D 72, 179. https://doi.org/10.1140/epjd/e2018-90138-3.

Ebele, A.J., Abou-Elwafa Abdallah, M., Harrad, S., 2017. Pharmaceuticals and personal care products (PPCPs) in the freshwater aquatic environment. Emerg. Contam. 3, 1–16. https://doi.org/10.1016/j.emcon.2016.12.004.

Eggen, R.I.L., Hollender, J., Joss, A., Schärer, M., Stamm, C., 2014. Reducing the discharge of micropollutants in the aquatic environment: the benefits of upgrading wastewater treatment plants. Environ. Sci. Technol. 48, 7683–7689. https://doi.org/10.1021/es500907n.

Foster, J., Sommers, B.S., Gucker, S.N., Blankson, I.M., Adamovsky, G., 2012. Perspectives on the interaction of plasmas with liquid water for water purification. IEEE Trans. Plasma Sci. 40, 1311–1323. https://doi.org/10.1109/TPS.2011.2180028.

Foster, J.E., 2017. Plasma-based water purification: challenges and prospects for the future. Phys. Plasmas 24, 055501. https://doi.org/10.1063/1.4977921.

Fridman, A., 2008. Plasma Chemistry. 1st Editio. ed. Cambridge University Press, Cambridge https://doi.org/10.1017/CBO9780511546075.

García, M.C., Mora, M., Esquivel, D., Foster, J.E., Rodero, A., Jiménez-Sanchidrián, C., Romero-Salguero, F.J., 2017. Microwave atmospheric pressure plasma jets for wastewater treatment: degradation of methylene blue as a model dye. Chemosphere 180, 239–246. https://doi.org/10.1016/j.chemosphere.2017.03.126.

Garrido-Cardenas, J.A., Esteban-García, B., Agüera, A., Sánchez-Pérez, J.A., Manzano-Agugliaro, F., 2020. Wastewater treatment by advanced oxidation process and their worldwide research trends. Int. J. Environ. Res. Public Health 17, 170. https://doi.org/10.3390/ijerph17010170.

Gazeli, K., Svarnas, P., Held, B., Marlin, L., Clément, F., 2015. Possibility of controlling the chemical pattern of He and Ar “guided streamers” by means of N2 or O2 additives. J. Appl. Phys. 117, 093302. https://doi.org/10.1063/1.4914035.

Ghimire, B., Szili, E.J., Patenall, B.L., Lamichhane, P., Gaur, N., Robson, A.J., Trivedi, D., Thet, N.T., Jenkins, A.T.A., Choi, E.H., Short, R.D., 2021. Enhancement of hydrogen peroxide production from an atmospheric pressure argon plasma jet and implications to the antibacterial activity of plasma activated water. Plasma Sources Sci. Technol. 30, 035009. https://doi.org/10.1088/1361-6595/abe0c9.

He, Y., Grieser, F., Ashokkumar, M., 2011. Kinetics and mechanism for the sonophotocatalytic degradation of p -chlorobenzoic acid. J. Phys. Chem. A 115, 6582–6588. https://doi.org/10.1021/jp203518s.

Heberer, T., Feldmann, D., 2005. Contribution of effluents from hospitals and private households to the total loads of diclofenac and carbamazepine in municipal sewage effluents - modeling versus measurements. J. Hazard. Mater. 122, 211–218. https://doi.org/10.1016/j.jhazmat.2005.03.007.

Hijosa-Valsero, M., Molina, R., Montràs, A., Müller, M., Bayona, J.M., 2014. Decontamination of waterborne chemical pollutants by using atmospheric pressure nonthermal plasma: a review. Environ. Technol. Rev. 3, 71–91. https://doi.org/10.1080/21622515.2014.990935.

Invernizzi, L., Muja, C., Sainct, F.P., Guillot, P., 2020. Investigation of RONS production and complex molecules degradation induced by an APPJ generated by two different sources. IEEE Trans. Radiat. Plasma Med. Sci. 4, 121–129. https://doi.org/10.1109/TRPMS.2019.2918623.

Jaiswal, A.K., Ananthanarasimhan, J., Shivapuji, A.M., Dasappa, S., Rao, L., 2020. Experimental investigation of a non-catalytic cold plasma water-gas shift reaction. J. Phys. D. Appl. Phys. 53, 465205. https://doi.org/10.1088/1361-6463/aba92d.

Jaiswal, S., Aguirre, E.M., 2021. Comparison of atmospheric pressure argon producing O(1S) and helium plasma jet on methylene blue degradation. AIP Adv. 11, 045311. https://doi.org/10.1063/5.0046948.

Jankunaite, D., Tichonovas, M., Buivydiene, D., Radziuniene, I., Racys, V., Krugly, E., 2017. Removal of diclofenac, ketoprofen, and carbamazepine from simulated drinking water by advanced oxidation in a model reactor. Water Air Soil Pollut. 228, 1–15. https://doi.org/10.1007/s11270-017-3517-z.

Judée, F., Simon, S., Bailly, C., Dufour, T., 2018. Plasma-activation of tap water using DBD for agronomy applications: identification and quantification of long lifetime chemical species and production/consumption mechanisms. Water Res. 133, 47–59. https://doi.org/10.1016/j.watres.2017.12.035.

Khan, N.A., Ahmed, S., Farooqi, I.H., Ali, I., Vambol, V., Changani, F., Yousefi, M., Vambol, S., Khan, S.U., Khan, A.H., 2020. Occurrence, sources and conventional treatment techniques for various antibiotics present in hospital wastewaters: a critical review. TrAC Trends Anal. Chem. 129, 115921. https://doi.org/10.1016/j.trac.2020.115921.

Kot-Wasik, A., Debska, J., Namieśnik, J., 2007. Analytical techniques in studies of the environmental fate of pharmaceuticals and personal-care products. TrAC, Trends Anal. Chem. 26, 557–568. https://doi.org/10.1016/j.trac.2006.11.004.

Kumar, A., Škoro, N., Gernjak, W., Povrenović, D., Puač, N., 2022. Direct and indirect treatment of organic dye (Acid blue 25) solutions by using cold atmospheric plasma jet. Front. Phys. 10, 1–14. https://doi.org/10.3389/fphy.2022.835635.

Kumar, A., Škoro, N., Gernjak, W., Puač, N., 2021. Cold atmospheric plasma technology for removal of organic micropollutants from wastewater—a review. Eur. Phys. J. D 75, 1–26. https://doi.org/10.1140/epjd/s10053-021-00283-5.

Lamichhane, P., Acharya, T.R., Kaushik, N., Nguyen, L.N., Lim, J.S., Hessel, V., Kaushik, N.K., Choi, E.H., 2022. Non-thermal argon plasma jets of various lengths for selective reactive oxygen and nitrogen species production. J. Environ. Chem. Eng. 10, 107782. https://doi.org/10.1016/j.jece.2022.107782.

Lesage, O., Falk, L., Tatoulian, M., Mantovani, D., Ognier, S., 2013. Treatment of 4-chlorobenzoic acid by plasma-based advanced oxidation processes. Chem. Eng. Process. Process Intensif. 72, 82–89. https://doi.org/10.1016/j.cep.2013.06.008.

Lesage, O., Roques-Carmes, T., Commenge, J.M., Duten, X., Tatoulian, M., Cavadias, S., Mantovani, D., Ognier, S., 2014. Degradation of 4-chlorobenzoïc acid in a thin falling film dielectric barrier discharge reactor. Ind. Eng. Chem. Res. 53, 10387–10396. https://doi.org/10.1021/ie403772t.

Li, S., Ma, X., Jiang, Y., Cao, X., 2014. Acetamiprid removal in wastewater by the low-temperature plasma using dielectric barrier discharge. Ecotoxicol. Environ. Saf. 106, 146–153. https://doi.org/10.1016/j.ecoenv.2014.04.034.

Liu, F., Liang, J., Chen, L., Tong, M., Liu, W., 2019. Photocatalytic removal of diclofenac by ti doped BiOI microspheres under visible light irradiation: kinetics, mechanism, and pathways. J. Mol. Liq. 275, 807–814. https://doi.org/10.1016/j.molliq.2018.11.119.

Liu, J., He, B., Chen, Q., Li, J., Xiong, Q., Yue, G., Zhang, X., Yang, S., Liu, H., Liu, Q.H., 2016. Direct synthesis of hydrogen peroxide from plasma-water interactions. Sci. Rep. 6, 1–7. https://doi.org/10.1038/srep38454.

Lonappan, L., Brar, S.K., Das, R.K., Verma, M., Surampalli, R.Y., 2016. Diclofenac and its transformation products: environmental occurrence and toxicity - a review. Environ. Int. 96, 127–138. https://doi.org/10.1016/j.envint.2016.09.014.

Lukes, P., Dolezalova, E., Sisrova, I., Clupek, M., 2014. Aqueous-phase chemistry and bactericidal effects from an air discharge plasma in contact with water: evidence for the formation of peroxynitrite through a pseudo-second-order post-discharge reaction of H2O2 and HNO2. Plasma Sources Sci. Technol. 23, 015019. https://doi.org/10.1088/0963-0252/23/1/015019.

Lukes, P., Locke, B.R., Brisset, J., 2012. Aqueous-phase chemistry of electrical discharge plasma in water and in gas–liquid environments. Plasma Chemistry and Catalysis in Gases and Liquids. Wiley, pp. 243–308 https://doi.org/10.1002/9783527649525.ch7.

Ma, D., Yi, H., Lai, C., Liu, X., Huo, X., An, Z., Li, L., Fu, Y., Li, B., Zhang, M., Qin, L., Liu, S., Yang, L., 2021. Critical review of advanced oxidation processes in organic wastewater treatment. Chemosphere 275, 130104. https://doi.org/10.1016/j.chemosphere.2021.130104.

Macías-Quiroga, I.F., Henao-Aguirre, P.A., Marín-Flórez, A., Arredondo-López, S.M., Sanabria-González, N.R., 2021. Bibliometric analysis of advanced oxidation processes (AOPs) in wastewater treatment: global and ibero-american research trends. Environ. Sci. Pollut. Res. 28, 23791–23811. https://doi.org/10.1007/s11356-020-11333-7.

Magureanu, M., Mandache, N.B., Parvulescu, V.I., 2015. Degradation of pharmaceutical compounds in water by non-thermal plasma treatment. Water Res. 81, 124–136. https://doi.org/10.1016/j.watres.2015.05.037.

Malik, M.A., 2010. Water purification by plasmas: which reactors are most energy efficient? Plasma Chem. Plasma Process. 30, 21–31. https://doi.org/10.1007/s11090-009-9202-2.

Markandya, A., Taylor, T., Longo, A., Murty, M.N., Murty, S., Dhavala, K., 2008. Counting the cost of vulture decline-an appraisal of the human health and other benefits of vultures in India. Ecol. Econ. 67, 194–204. https://doi.org/10.1016/j.ecolecon.2008.04.020.

Monteagudo, J.M., El-taliawy, H., Durán, A., Caro, G., Bester, K., 2018. Sono-activated persulfate oxidation of diclofenac: degradation, kinetics, pathway and contribution of the different radicals involved. J. Hazard. Mater. 357, 457–465. https://doi.org/10.1016/j.jhazmat.2018.06.031.

Mukherjee, A.G., Wanjari, U.R., Eladl, M.A., El-Sherbiny, M., Elsherbini, D.M.A., Sukumar, A., Kannampuzha, S., Ravichandran, M., Renu, K., Vellingiri, B., Kandasamy, S., Gopalakrishnan, A.V., 2022. Mixed contaminants: occurrence, interactions, toxicity, detection, and remediation. Molecules 27, 2577. https://doi.org/10.3390/molecules27082577.

Patel, M., Kumar, R., Kishor, K., Mlsna, T., Pittman, C.U., Mohan, D., 2019. Pharmaceuticals of emerging concern in aquatic systems: chemistry, occurrence, effects, and removal methods. Chem. Rev. 119, 3510–3673. https://doi.org/10.1021/acs.chemrev.8b00299.

Pawłat, J., Terebun, P., Kwiatkowski, M., Tarabová, B., Kovaľová, Z., Kučerová, K., Machala, Z., Janda, M., Hensel, K., 2019. Evaluation of oxidative species in gaseous and liquid phase generated by mini-gliding arc discharge. Plasma Chem. Plasma Process. 39, 627–642. https://doi.org/10.1007/s11090-019-09974-9.

Peng, Y., Shi, H., Wang, Z., Fu, Y., Liu, Y., 2021. Kinetics and reaction mechanism of photochemical degradation of diclofenac by UV-activated peroxymonosulfate. RSC Adv. 11, 6804–6817. https://doi.org/10.1039/D0RA10178H.

Phatak, P.V., Gaikar, V.G., 1996. Solubilities of o-and p-chlorobenzoic acids and o-and p-nitroanilines in N, N-Dimethylformamide + Water. J. Chem. Eng. Data 41, 1052–1054. https://doi.org/10.1021/je9600820.

Pi, Y., Schumacher, J., Jekel, M., 2005. The use of Para-chlorobenzoic acid (pCBA) as an ozone/hydroxyl radical probe compound. Ozone Sci. Eng. 27, 431–436. https://doi.org/10.1080/01919510500349309.

Rezaei, F., Vanraes, P., Nikiforov, A., Morent, R., Geyter, N.De, 2019. Applications of plasma-liquid systems : a review. Materials 12, 2751. https://doi.org/10.3390/ma12172751.

Rodrigues, J.A., Silva, S., Cardoso, V.V., Benoliel, M.J., Cardoso, E., Coelho, M.R., Martins, A., Almeida, C.M.M., 2021. Screening and seasonal behavior of analgesics, non-steroidal anti-inflammatory drugs, and antibiotics in two urban wastewater treatment plants. Environ. Manag. 68, 411–425. https://doi.org/10.1007/s00267-021-01496-5.

Rong, S., Sun, Y., Zhao, Z., Wang, H., 2014. Dielectric barrier discharge induced degradation of diclofenac in aqueous solution. Water Sci. Technol. 69, 76–83. https://doi.org/10.2166/wst.2013.554.

Salgado, R., Pereira, V.J., Carvalho, G., Soeiro, R., Gaffney, V., Almeida, C., Cardoso, V.V., Ferreira, E., Benoliel, M.J., Ternes, T.A., Oehmen, A., Reis, M.A.M., Noronha, J.P., 2013. Photodegradation kinetics and transformation products of ketoprofen, diclofenac and atenolol in pure water and treated wastewater. J. Hazard. Mater. 244–245, 516–527. https://doi.org/10.1016/j.jhazmat.2012.10.039.

Sathishkumar, P., Meena, R.A.A., Palanisami, T., Ashokkumar, V., Palvannan, T., Gu, F.L., 2020. Occurrence, interactive effects and ecological risk of diclofenac in environmental compartments and biota - a review. Sci. Total Environ. 698, 134057. https://doi.org/10.1016/j.scitotenv.2019.134057.

Schellenberg, T., Subramanian, V., Ganeshan, G., Tompkins, D., Pradeep, R., 2020. Wastewater discharge standards in the evolving context of urban sustainability-the case of India. Front. Environ. Sci. 8. https://doi.org/10.3389/fenvs.2020.00030.

Schönekerl, S., Weigert, A., Uhlig, S., Wellner, K., Pörschke, R., Pfefferkorn, C., Backhaus, K., Lerch, A., 2020. Evaluating the performance of a lab-scale water treatment plant using non-thermal plasma technology. Water 12, 1956. https://doi.org/10.3390/w12071956.

Schwarzenbach, R.P., Escher, B.I., Fenner, K., Hofstetter, T.B., Johnson, C.A., von Gunten, U., Wehrli, B., 2006. The challenge of micropollutants in aquatic systems. Science 313, 1072–1077. https://doi.org/10.1126/science.1127291.

Soler-Arango, J., Brelles-Mariño, G., Rodero, A., Garcia, M.C., 2018. Characterization of an air-based coaxial dielectric barrier discharge plasma source for biofilm eradication. Plasma Chem. Plasma Process. 38, 535–556. https://doi.org/10.1007/s11090-018-9877-3.

Taggart, M.A., Senacha, K.R., Green, R.E., Cuthbert, R., Jhala, Y.V., Meharg, A.A., Mateo, R., Pain, D.J., 2009. Analysis of nine NSAIDs in ungulate tissues available to critically endangered vultures in India. Environ. Sci. Technol. 43, 4561–4566. https://doi.org/10.1021/es9002026.

Thirumdas, R., Kothakota, A., Annapure, U., Siliveru, K., Blundell, R., Gatt, R., Valdramidis, V.P., 2018. Plasma activated water (PAW): chemistry, physico-chemical properties, applications in food and agriculture. Trends Food Sci. Technol. 77, 21–31. https://doi.org/10.1016/j.tifs.2018.05.007.

Tomić, S., Petrović, A., Puač, N., Škoro, N., Bekić, M., Petrović, Z.L., Čolić, M., 2021. Plasma-activated medium potentiates the immunogenicity of tumor cell lysates for dendritic cell-based cancer vaccines. Cancers 13, 10–13. https://doi.org/10.3390/cancers13071626.

Topolovec, B., Škoro, N., Puač, N., Petrovic, M., 2022. Pathways of organic micropollutants degradation in atmospheric pressure plasma processing – a review. Chemosphere 294, 133606. https://doi.org/10.1016/j.chemosphere.2022.133606.

Uhm, H.S., Ki, S.H., Baik, K.Y., Choi, E.H., 2018. Influence of oxygen on generation of reactive chemicals from nitrogen plasma jet. Sci. Rep. 8, 1–12. https://doi.org/10.1038/s41598-018-27473-3.

Wang, J.L., Xu, L.J., 2012. Advanced oxidation processes for wastewater treatment: formation of hydroxyl radical and application. Crit. Rev. Environ. Sci. Technol. 42, 251–325. https://doi.org/10.1080/10643389.2010.507698.

Wenjuan, B., Xiangli, Y., 2007. Nitrogen fixation into HNO3 and HNO2 by pulsed high voltage discharge. Plasma Sci. Technol. 9, 288–291. https://doi.org/10.1088/1009-0630/9/3/08.

Wilkinson, J.L., Boxall, A.B.A., Al, K., 2022. Pharmaceutical pollution of the world's rivers. Proceedings of the National Academy of Sciences 119, 1–10. https://doi.org/10.1073/pnas.2113947119.

Xiong, R., Xiong, Q., Nikiforov, A.Y., Vanraes, P., Leys, C., 2012. Influence of helium mole fraction distribution on the properties of cold atmospheric pressure helium plasma jets. J. Appl. Phys. 112, 033305. https://doi.org/10.1063/1.4746700.

Yehia, S.A., Zarif, M.E., Bita, B.I., Teodorescu, M., Carpen, L.G., Vizireanu, S., Petrea, N., Dinescu, G., 2020. Development and optimization of single filament plasma jets for wastewater decontamination. Plasma Chem. Plasma Process. 40, 1485–1505. https://doi.org/10.1007/s11090-020-10111-0.

Yousfi, M., Merbahi, N.P.J., Eichwald, O., Ricard, A., Gardou, J.P., Ducasse, O., Benhenni, M., 2011. Non thermal plasma sources of production of active species for biomedical uses: analyses, optimization and prospect. Biomedical Engineering - Frontiers and Challenges https://doi.org/10.5772/19129.

Zhang, L., Liu, Y., Fu, Y., 2020. Degradation kinetics and mechanism of diclofenac by UV/peracetic acid. RSC Adv. 10, 9907–9916. https://doi.org/10.1039/d0ra00363h.